

FSTF SHELL CONDENSATION
OSCILLATION LOADING CORRECTION
FACTORS - UNCORRELATED VENTS

Revision 2

by

D. B. Bliss and M. E. Teske

Continuum Dynamics, Inc.
32 Nassau Street
P.O. Box 3073
Princeton, New Jersey 08540

for

Nuclear Energy Division
General Electric Company
175 Curtner Avenue
San Jose, California 95125

under

Purchase Order 205-XC911

Approved



Alan J. Bilanin
President

AUGUST 1980

9110070196 910927
PDR ADOCK 05000220
P PDR

2
3
4
5
6
7
8
9
10
11
12



TABLE OF CONTENTS

SECTION	TITLE	PAGE
	Nomenclature	i
	Executive Summary	iii
I.	Introduction	1
II.	Examination of the Random Nature of FSTF Shell Loading	2
III.	Analysis of the Effects of Vent Correlation on Pressure Loads in FSTF	5
IV.	Calculation of the PSD Load Reduction Factors in FSTF	25
V.	Effect of Partial Correlation Between Vents	29



1
2
3
4
5
6
7
8
9
10
11
12
13
14
15
16
17
18
19
20
21
22
23
24
25
26
27
28
29
30
31
32
33
34
35
36
37
38
39
40
41
42
43
44
45
46
47
48
49
50
51
52
53
54
55
56
57
58
59
60
61
62
63
64
65
66
67
68
69
70
71
72
73
74
75
76
77
78
79
80
81
82
83
84
85
86
87
88
89
90
91
92
93
94
95
96
97
98
99
100

NOMENCLATURE

a	radius of cylindrical torus
c	acoustic speed
c_n	series parameter defined in Equation 10
d	section length along a torus
D	half-length of a cylinder
$(\vec{e}_r, \vec{e}_\theta, \vec{e}_z)$	unit vectors in (r, θ , z) directions
f	frequency in Hz
F	transfer function
H	frequency response function
J_n	Bessel function
ℓ	segment length
λ_v	distance between segment stations
L	torus half-circumference length
m_n^j	jth stationary value of J_n , defined in Equation 5
n_s	number of segment circumferential stations
n_v	number of vents at each segment station
N	number of linear segments in a torus
p, P	pressure
q	normalized source strength, defined in Equation 35
\vec{q}	total velocity vector
Q	volume flow rate
r	radius
(r_v, θ_v, z_v)	cylindrical polar coordinates measured from a vent source
R	cross-correlation function
R_F	load reduction factor
S	power spectral density



t	time
(u,v,w)	velocity components in (r,θ,z) directions
z	distance along torus
α_n	wave solution parameter, defined in Equation 4
δ	Dirac delta function
θ	angle
ξ	coordinate transformation variable
ρ	density
ρ_c, ρ_{ij}	correlation coefficient
ω	frequency in radians/sec

SUPERSCRIPTS

$(\bar{\quad})$	time average
$(\hat{\quad})$	FSTF configuration
$(\tilde{\quad})$	modified time average



Vertical text or markings on the left side of the page, possibly bleed-through from the reverse side.

EXECUTIVE SUMMARY

An analysis of measured downcomer pressure data in FSTF Run M8 was undertaken in the 0 - 50 Hz frequency range during condensation oscillation to assess the degree of randomness inherent in the vent dynamics. Correlation coefficients generated for these data indicate that the sources at the exits of the vents in the 0 - 50 Hz frequency range are random and uncorrelated except at 5 Hz and the 8 - 10 Hz frequency range, where the signals are strongly correlated. Condensation oscillation load reduction factors are developed which may be used to adjust FSTF PSD's of average shell pressure data to take credit for source randomization between vents and bays. It is shown that the PSD's of measured average bottom pressure data are conservative by nearly a factor of two (except at 5 Hz and the 8 - 10 Hz frequency range), without taking credit for reduced sound speed in water. The data is even more conservative for lower acoustic speeds in water. Correlation of the vent sources is shown to partially negate the PSD reduction factors. The PSD reduction factors which form the major result of this study are summarized in Figures 9 and 10.



Vertical text on the left side, possibly a page number or header, appearing as a series of small, dark, illegible characters.

Faint, illegible text or markings in the center of the page.

I. INTRODUCTION

Examination of the correlation coefficients of FSTF downcomer pressure histories in the 0 - 50 frequency range during condensation oscillation indicates a lack of coherence among the condensation processes at the vent exits for most of this frequency range. Therefore, as a consequence of the "rigid" end caps installed in FSTF to end the bay, shell loadings measured in FSTF will be higher than loadings measured in a prototypical plant. This is because, in FSTF, loads are measured as if all other bays are exactly in phase or are coherent with the bay modeled by FSTF. By demonstrating that in a given frequency range vents and hence bays are necessarily uncorrelated, load reduction factors may be developed to take credit for lack of coherence between bays. In this report an analysis of 15 seconds of FSTF Run M8, in the time interval 20 - 35 seconds of condensation oscillation data involving pressure transducers P5323, P5443, P5523, P5643, P5723 and P5843 on downcomers 3 through 8, is undertaken. Correlation coefficients are generated as a function of frequency for each unique pair of pressure signals. An analysis is then undertaken to develop load reduction factors which may be applied to the PSD's of the shell pressure field over the signal frequency range. Finally, the effect of correlation on the resultant PSD reduction factors is discussed.



II. EXAMINATION OF THE RANDOM NATURE OF FSTF SHELL LOADING

The mean square pressure signal at a containment wall from two vents with pressures $P_i(t)$ and $P_j(t)$ is given by

$$\overline{(P_i + P_j)^2} = \overline{P_i^2} + 2\overline{P_i P_j} + \overline{P_j^2}$$

where the overbar denotes a time average. If P_i and P_j are random and incoherent, then $\overline{P_i P_j} = 0$, ($i \neq j$), and the correlation coefficient between the two vents is defined to be

$$\rho_c = \rho_{ij} = \frac{\overline{P_i P_j}}{\sqrt{\overline{P_i^2}} \sqrt{\overline{P_j^2}}} = 0$$

Thus the correlation $\overline{P_i P_j}$ indicates the amount of correlation in the signals from the two vents.

For the time period 20 - 35 seconds for FSTF run M8, the data from transducers on downcomers 3 through 8 near their exits was Fourier decomposed and then used to construct the mean square pressure signal components $\overline{(P_i + P_j)^2}$, $\overline{P_i^2} + \overline{P_j^2}$ and $\overline{P_i P_j}$ for each of the 15 unique downcomer pair combinations. These mean square quantities are calculated as a function band width with the band always starting at zero frequency (DC). As the higher frequency contributions are added to the signals, the amount of downcomer correlation is estimated by large rates of change with frequency of the $\overline{P_i P_j}$ signal. A representative result is shown in Figure 1 for the 0 - 50 Hz frequency range. Here the rapid rate of change in $\overline{P_5 P_6}$ near 5 Hz, and a smaller change between 8 and 10 Hz, with perhaps a slight change at 17 Hz, indicate that these frequency regions are where the downcomer pressure signals during condensation oscillation are correlated. Figure 1 indicates that apart from these particular regions, and certainly for frequencies above 20 Hz, the correlation coefficient is well approximated by zero.



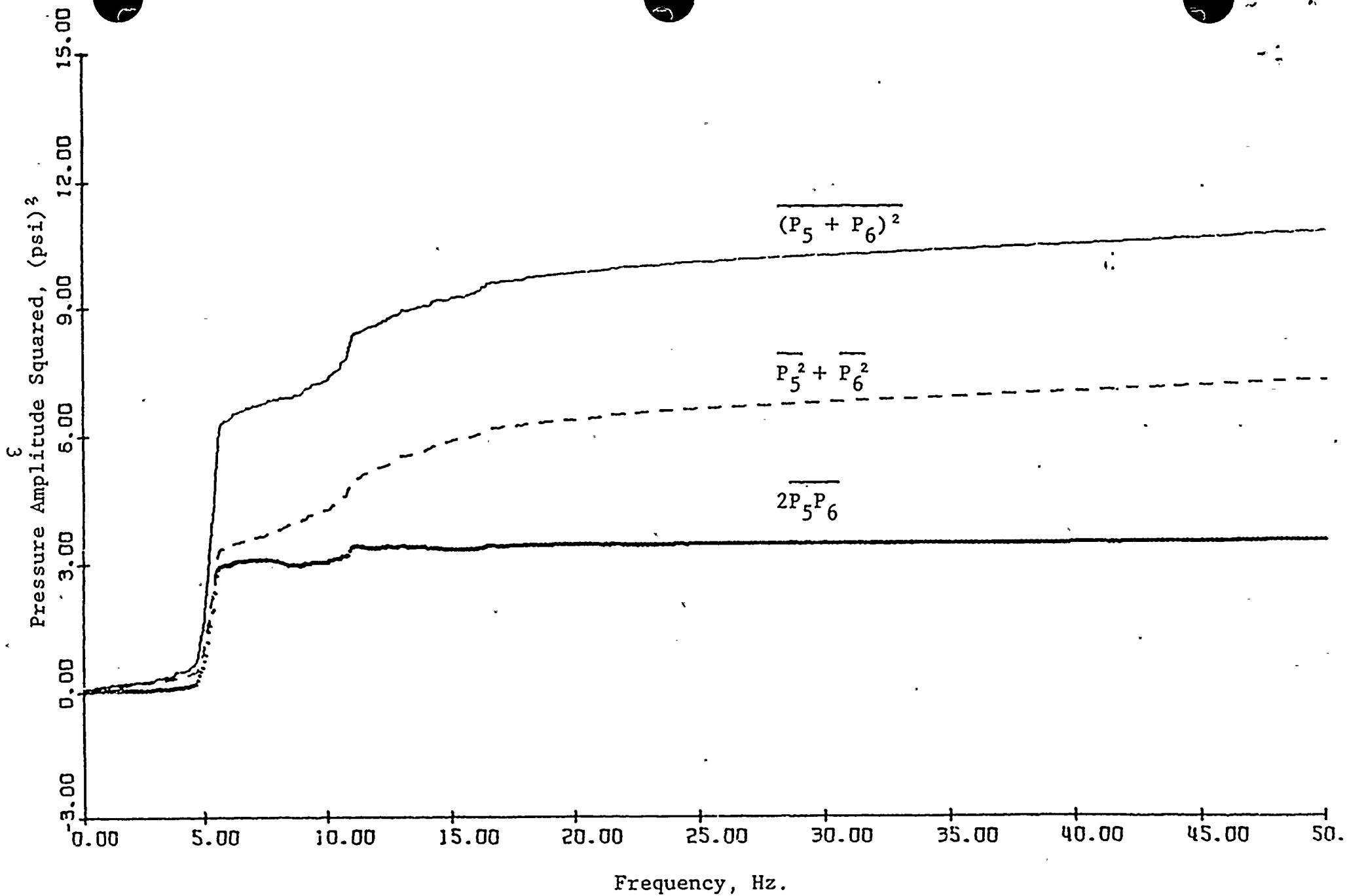


Figure 1: Mean Square pressure signals between downcomers 5 and 6, FSTF Run M8, 20 - 35 seconds, during condensation oscillation as a function of frequency bandwidth (measured from zero frequency)



Vertical text on the left side of the page, possibly bleed-through from the reverse side.

Small mark or character.

Thus, since the condensation process at each vent is random and uncorrelated, the shell loading in a torus will be other than what is measured in FSTF because of the perfect reflection effect of the rigid wall end caps installed in the FSTF. A methodology is developed below to quantify the amount of conservatism which exists in the Mark I Condensation Oscillation loads as a consequence of the end cap effect.

One can speculate as to the origin of this random signal. Condensation oscillation is described as the highly periodic growth and collapse of a steam bubble at the exit of the vent. While the growth process has been observed to be closely in-phase among all vents, the collapse process (in particular, the final stages of collapse) is not. Apparently, local pool turbulence, steam water interface instabilities and buoyancy all contribute to the detailed collapse at the vent exit. It would not be surprising to find that the final stages of collapse are random and that the distribution of sizes of steam/air bubbles left in the pool are also random. An estimation of the bubble sizes required to produce a signal in the 20-50 Hz frequency range is consistent with what might be expected to occur at the vent exit.



Vertical text on the left side, possibly a page number or header, appearing as a column of small, dark characters.

Main body of text in the center, consisting of several lines of faint, illegible characters.

III. ANALYSIS OF THE EFFECTS OF VENT CORRELATION ON PRESSURE LOADS IN FSTF

CONFIGURATION AND ASSUMPTIONS

Pressure pulsations occur as steam vents discharge beneath the water surface in a large half-filled toroidal vessel. The "torus" is of circular cross-section, with radius "a", and is constructed of "N" linear segments each having a centerline length " ℓ ". The half-circumference is defined as $L = \frac{1}{2}N\ell$. In each segment, there are " n_s " circumferential stations, each separated by a distance " ℓ_v ", with " n_v " vents located at each station. The pressure pulsations produce net vertical unsteady forces on the torus. The magnitude of these forces depends on the degree to which the pulsations from the various vent sources are correlated or uncorrelated. Unsteady loads were measured in a full scale test facility (FSTF) which resembles a portion of the torus enclosed by rigid end walls. It is desired to be able to transfer these test results to a full torus configuration, taking into account the different boundary conditions and the possible effects of source correlation.

In the analysis that follows, the pressure disturbances in the liquid are assumed to be governed by the simple wave equation. The walls of the vessel are assumed to be rigid and the water surface is modeled as a simple constant pressure boundary condition (therefore, gravitational waves are excluded). The torus is unwrapped and analyzed as a simple cylindrical geometry, so that the effects of curvature around the toroidal circumference are neglected. The fact that the torus closes on itself is taken into account through use of the proper boundary condition. The vents are modeled as simple point sources (delta functions) so that the local flow structure around the vent is ignored and only the net effect of mass addition and removal is considered. These assumptions lead to considerable simplifications in the analysis while still retaining the basic physics of interest and assuring a reasonable degree of computational accuracy.



FORMULATION FOR THE PRESSURE

The basis for the analysis is the solution of the wave equation in the half-filled cylinder of half-length "D" and radius "a", with cylindrical polar coordinates located as shown in Figure 2. A single vent source is located at the coordinates $(r_v, \theta_v, z=0)$. The distance "d" is a section length used to compute a net vertical force due to the unsteady pressure. The governing equation for the pressure is

$$\frac{\partial^2 p}{\partial r^2} + \frac{1}{r} \frac{\partial p}{\partial r} + \frac{1}{r^2} \frac{\partial^2 p}{\partial \theta^2} + \frac{\partial^2 p}{\partial z^2} - \frac{1}{c^2} \frac{\partial^2 p}{\partial t^2} = 0 \quad (1)$$

The associated boundary conditions for the geometry of Figure 2 are:

$$p(r, 0, z, t) = p(r, \pi, z, t) = 0 \quad 0 \leq r \leq a, \quad 0 \leq z \leq D \quad (\text{free surface})$$

$$\frac{\partial}{\partial r} p(a, \theta, z, t) = 0 \quad 0 \leq \theta \leq \pi, \quad 0 \leq z \leq D \quad (\text{hard wall})$$

$$\frac{\partial}{\partial z} p(r, \theta, D, t) = 0 \quad 0 \leq r \leq a, \quad 0 \leq \theta \leq \pi \quad (\text{hard wall}) \quad (2)$$

Using the method of separation of variables, the following general solution for harmonic time dependence is obtained:

$$p(r, \theta, z, t) = e^{i\omega t} \sum_{n=1}^{\infty} \sum_{j=1}^{\infty} c_{nj} J_n(m_n^j \frac{r}{a}) \sin n\theta \frac{\cosh[\alpha_{nj}(D-z)]}{\cosh[\alpha_{nj}D]} \quad (3)$$

where

$$\alpha_{nj} = \frac{1}{a} \sqrt{(m_n^j)^2 - (\frac{\omega a}{c})^2} \quad (4)$$

The quantity m_n^j is defined to be the j^{th} stationary value of the Bessel function J_n , namely

$$\frac{d}{dr} J_n(m_n^j) = 0 \quad (5)$$

where, for instance, $m_1^1 = 1.84118$, $m_1^2 = 5.33144$, etc.

The form of the pressure as expressed by Eqs. (3) and (4) assumes



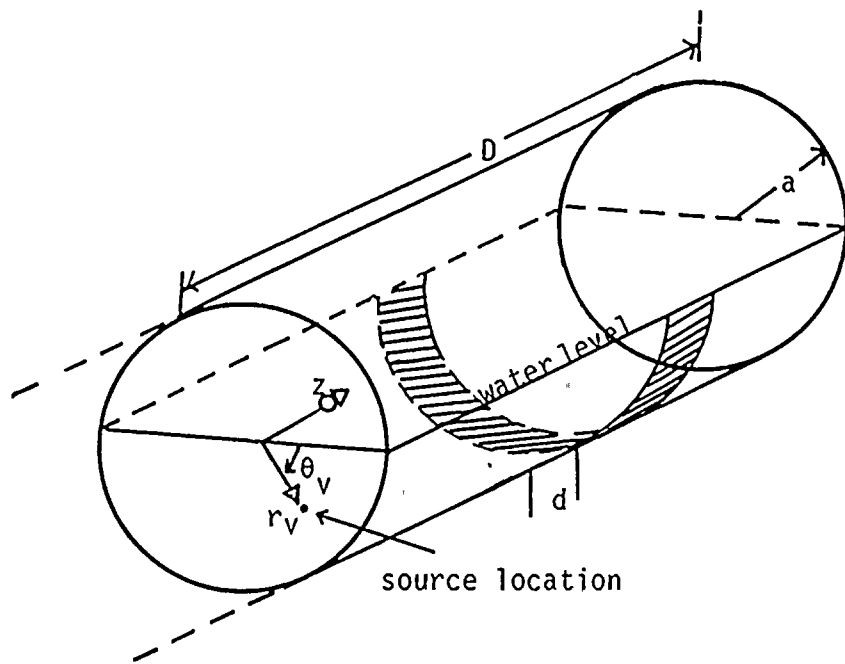


Figure 2. Basic Geometry for Calculating the Pressure.



Vertical text on the left side, possibly a page number or header, including characters like '第' and '頁'.

Small horizontal text fragment located in the lower-left quadrant of the page.

α_{nj} is real, namely $(\frac{\omega a}{c}) < m_n^j$. The solution is thus restricted to sufficiently low frequency that axial propagation of pressure disturbances does not occur. This is the case of physical interest, since if $a = 1\bar{4}$ ft and $c = 2500$ ft/sec the solution form is valid until a frequency $f = 52.33$ Hz. The solution above this frequency value has the property that pressure disturbances decay, essentially exponentially, away from the vent and are everywhere in phase.

The general solution will be specialized to the case of a single vent located at $(r_v, \theta_v, 0)$. The velocity field $\vec{q} = u\vec{e}_r + v\vec{e}_\theta + w\vec{e}_z$ can be calculated from the linearized momentum equation. For harmonic time dependence the z-component of velocity is

$$w = \frac{i}{\rho\omega} \frac{\partial p}{\partial z} \quad (6)$$

Substituting the general solution gives

$$w(r, \theta, z, t) = -\frac{ie^{i\omega t}}{\rho\omega} \sum_{n=1}^{\infty} \sum_{j=1}^{\infty} c_{nj} \alpha_{nj} J_n(m_n^j \frac{r}{a}) \sin n\theta \frac{\sinh[\alpha_{nj}(D-z)]}{\cosh(\alpha_{nj}D)} \quad (7)$$

Now let the net volume flow rate from a vent be $Qe^{i\omega t}$. Since this quantity must equal the net volume flow through a cross-sectional plane located at $z = 0+$, the z-component of velocity due to the vent must be

$$w(r, \theta, 0+, t) = \frac{Q}{2r_v a} \delta(\frac{r}{a} - \frac{r_v}{a}) \delta(\theta - \theta_v) e^{i\omega t} \quad (8)$$

The factor of two in the denominator is necessary because only half the volume flow goes in the positive z-direction. Equating Eqs. (7) and (8) and using the orthogonality properties of both trigonometric and Bessel functions permits the determination of the coefficients of the series in the general solution for pressure, Eq. (3). After a lengthy calculation, the result is:

$$p(r, \theta, z, t) = ie^{i\omega t} \frac{2\rho\omega Q}{\pi a^2} \sum_{n=1}^{\infty} \sum_{j=1}^{\infty} \hat{c}_{nj} \frac{J_n(m_n^j \frac{r}{a})}{J_n(m_n^j)} \sin n\theta \cosh[\alpha_{nj}(D-z)] \quad (9)$$



7214 4 2 1 2

17
22
23
24
25
26
27
28
29
30
31
32
33
34
35
36
37
38
39
40
41
42
43
44
45
46
47
48
49
50
51
52
53
54
55
56
57
58
59
60
61
62
63
64
65
66
67
68
69
70
71
72
73
74
75
76
77
78
79
80
81
82
83
84
85
86
87
88
89
90
91
92
93
94
95
96
97
98
99
100

7214 4 2 1 2

7214 4 2 1 2

where

$$\hat{c}_{nj} = \frac{\sin n\theta_v}{\alpha_{nj} \sinh[\alpha_{nj}D]} \frac{J_n(m_n^j \frac{r_v}{a})}{J_n(m_n^j)} \left[\frac{(m_n^j)^2}{(m_n^j)^2 - n^2} \right] \quad (10)$$

The root mean square (rms) pressure can be obtained directly from the above expression. The result is equivalent to replacing the pressure and volume flow with their rms values, \bar{p} and \bar{Q} respectively, and omitting the factor $ie^{i\omega t}$, which is of unit magnitude, in Eq. (9). Specifically, the rms wall pressure is given by

$$\bar{p}(a, \theta, z) = \frac{2\rho\omega\bar{Q}}{\pi a^2} \sum_{n=1}^{\infty} \sum_{j=1}^{\infty} \hat{c}_{nj} \sin n\theta \cosh[\alpha_{nj}(D-z)] \quad (11)$$

To compare with the experimental data, it is necessary to express the result as an area-averaged vertical component of the rms pressure, defined as follows

$$\bar{p}_{av} \equiv \frac{1}{2ad} \int_{z-d/2}^{z+d/2} \int_0^{\pi} \bar{p} \sin \theta a d\theta dz \quad \frac{d}{2} \leq z \leq D - \frac{d}{2} \quad (12)$$

The area "2ad" is the horizontal planform area of the shaded surface in Figure 2. The inequality condition is necessary to stay within the region of validity of the hyperbolic functions in the integrand. Substituting Eq. (11) into Eq. (12) gives the important result

$$\bar{p}_{av}(z) = \frac{\rho\omega\bar{Q}}{a^2 d} \sum_{j=1}^{\infty} K_j \cosh[\alpha_{1j}(D-z)] \quad \frac{d}{2} \leq z \leq D - \frac{d}{2} \quad (13)$$

where

$$K_j = \frac{\sin \theta_v}{\alpha_{1j}^2} \frac{\sinh(\alpha_{1j} \frac{d}{2})}{\sinh(\alpha_{1j} D)} \frac{J_1(m_1^j \frac{r_v}{a})}{J_1(m_1^j)} \left[\frac{(m_1^j)^2}{(m_1^j)^2 - 1} \right] \quad (14)$$

and, from Eq. (4),

$$\alpha_{1j} = \frac{1}{a} \sqrt{(m_1^j)^2 - (\frac{\omega a}{c})^2} \quad (15)$$

An interesting feature of the averaging process is that only the lowest circumferential harmonic ($n=1$) makes a net contribution to \bar{p}_{av} .



Vertical text on the left side, possibly a page number or header.

Vertical text on the left side, possibly a page number or header.

In parts of the analysis that follow, it is necessary to calculate the pressure contribution of a single source in the torus. Unfortunately, the inequality restriction on the argument "z" in Eq. (13) is very inconvenient in this case, since it prohibits certain relative locations of the source and the averaging area. It is therefore necessary to develop a more general expression without this restriction. Because the torus closes on itself, the pressure must be symmetric about both the source location and the reflection point half-way around the circumference. Setting $D = L$, the half-circumference, the definition of the pressure as given in Eq. (11) is extended as follows:

$$\begin{aligned}\bar{p}(a, \theta, z) &= \bar{p}(a, \theta, -z) \\ \bar{p}(a, \theta, L-\xi) &= \bar{p}(z, \theta, L+\xi)\end{aligned}\tag{16}$$

where $\xi = z-L$ is a coordinate with its origin at the reflection point. The averaging operation of Eq. (12) could be used now to obtain a vertical component of the rms pressure, \bar{p}_{av_L} , due to a single source averaged over a length d in the torus. Actually, the result can be developed more simply by a judicious application of Eq. (13). As shown in Figure 3, the symmetry of the torus causes the force on the area in the left-hand sketch to be the same as the sum of the forces on the two areas in the right-hand sketch. Using Eq. (13) to find the forces on these two areas, and adding the results to obtain the average vertical pressure for the entire averaging area gives:

$$\bar{p}_{av_L}(z) = \begin{cases} \tilde{p}_{av}(\frac{\tilde{d}}{2}) \Big|_{\tilde{d}=\frac{d}{2}+z} + \tilde{p}_{av}(\frac{\tilde{d}}{2}) \Big|_{\tilde{d}=\frac{d}{2}-z} & 0 \leq z < \frac{d}{2} \\ \bar{p}_{av}(z) \Big|_{D=L} & \frac{d}{2} \leq z \leq L-\frac{d}{2} \\ \tilde{p}_{av}(L - \frac{\tilde{d}}{2}) \Big|_{\tilde{d}=\frac{d}{2}+(L-z)} + \tilde{p}_{av}(L - \frac{\tilde{d}}{2}) \Big|_{\tilde{d}=\frac{d}{2}-(L-z)} & L-\frac{d}{2} < z \leq L \end{cases}\tag{17}$$



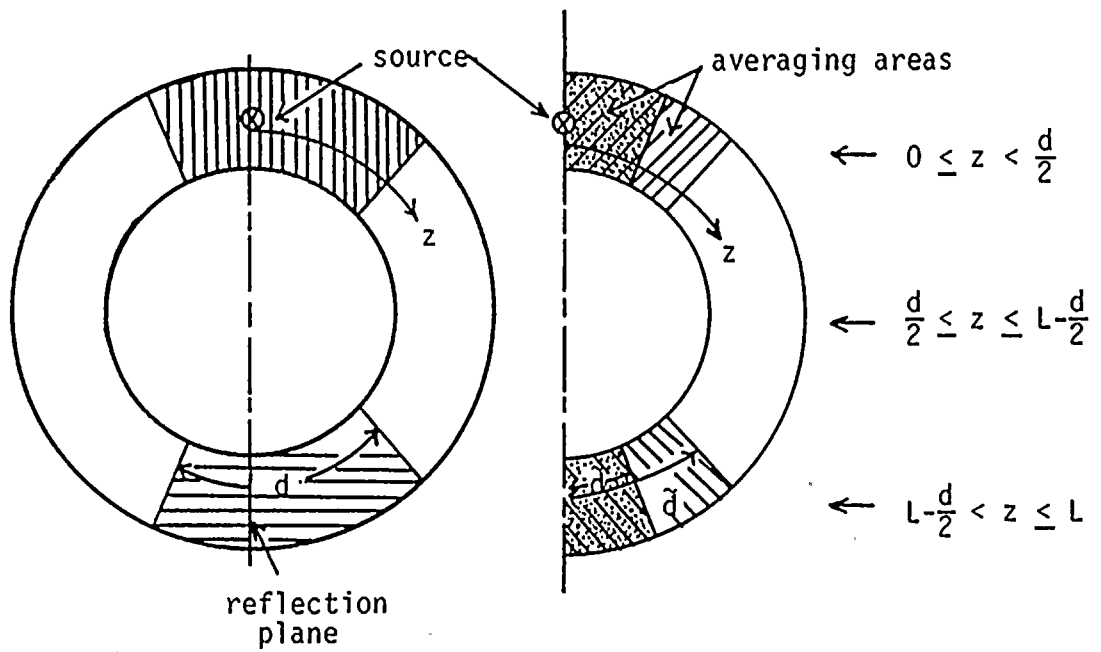


Figure 3. Geometry for Computing Average Pressure in a Torus.



The new function \tilde{p}_{av} is a modification of Eqs. (13) and (14) in accordance with the areas shown in Figure 3, namely

$$\tilde{p}_{av}(\eta) = \frac{\rho\omega\bar{Q}}{a^2d} \sum_{j=1}^{\infty} \tilde{K}_j \cosh[\alpha_{1j}(L-\eta)] \quad (18)$$

where

$$\tilde{K}_j = \frac{\sin \theta_v}{\alpha_{1j}^2} \frac{\sinh(\alpha_{1j} \frac{\tilde{d}}{2})}{\sinh(\alpha_{1j} L)} \frac{J_1(m_1^j \frac{r_v}{a})}{J_1(m_1^j)} \left[\frac{(m_1^j)^2}{(m_1^j)^2 - 1} \right] \quad (19)$$

Note that retaining the total averaging area "a²d" in Eq. (18) provides correct weighting for the additional pressure contributions in Eq. (17).

The approach to be taken, using the results just developed, will first be summarized. Depending on the geometry, Eq. (13) or Eq. (17) can be used to relate the average vertical pressure to the volume flow rate (of source strength \bar{Q}) of a single vent. Thus, these equations can be used to relate the net average vertical pressure to the source strength in containment configurations with multiple vents (correlated or uncorrelated), such as FSTF. This result is achieved by suitably defining the dimensions "d" and "D", and by adding the source contributions in the appropriate manner. Given the \bar{p}_{av} as a function of frequency (determined experimentally in FSTF), the corresponding function \bar{Q} can be determined, assuming either that all vent sources are correlated or uncorrelated. The function \bar{Q} can be used to predict \bar{p}_{av} as a function of frequency in a toroidal vessel, assuming correlated, partly correlated, or uncorrelated sources.

DETERMINATION OF VENT SOURCE STRENGTH

Case 1: All Vents Correlated

Let the notation $(\hat{\quad})$ denote the properties characterizing the FSTF. Figure 4 shows a schematic of the FSTF configuration which has a length " \hat{L} " between hard walls with $\hat{n}_v = 2$ vents at each of the $\hat{n}_s = 4$ vent stations. Assuming all vents are cor-



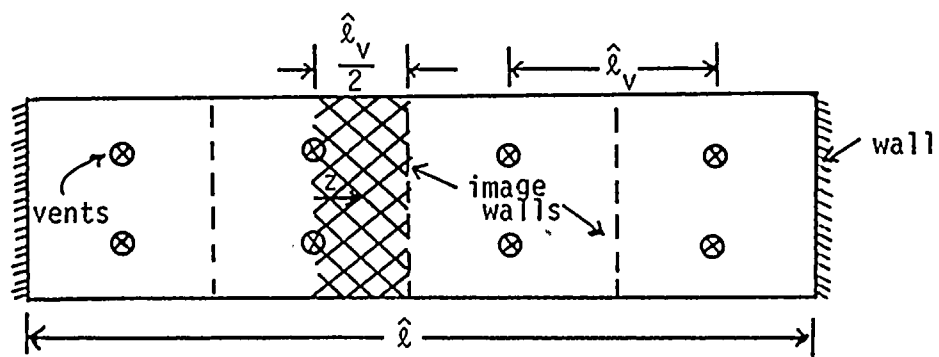


Figure 4. FSTF Geometry for Case 1: All Vents Correlated.



Vertical text on the left side, possibly a page number or header.

Vertical text on the left side, possibly a page number or header.

Vertical text on the left side, possibly a page number or header.

Vertical text on the left side, possibly a page number or header.

Vertical text on the left side, possibly a page number or header.

related, they form an image system equivalent to placing rigid walls at a distance $\hat{\lambda}_v/2$ on each side of a single vent pair. The average vertical pressure component is the same below each vent. Thus, \bar{p}_{av} is found using Eqs. (13) and (14) and setting $D = \hat{\lambda}_v/2$, $d = \hat{\lambda}_v/2$, $z = \hat{\lambda}_v/4$, corresponding to the cross-hatched area in Figure 4. Since there are two vents at each station, the experimentally measured pressure in the FSTF is actually $\bar{p}_x = 2\bar{p}_{av}$. Making the substitutions into Eqs. (13) and (14) and solving for the source strength gives

$$\bar{Q}_1 = \bar{p}_x \frac{\hat{\lambda}_v \hat{a}^2}{4\rho\omega} \left[\sum_{j=1}^{\infty} K_{j1} \cosh[\alpha_{1j} \frac{\hat{\lambda}_v}{4}] \right]^{-1} \quad (20)$$

where

$$K_{j1} = \frac{\sin \hat{\theta}_v}{\alpha_{1j}^2} \frac{\sinh[\alpha_{1j} \frac{\hat{\lambda}_v}{4}]}{\sinh[\alpha_{1j} \frac{\hat{\lambda}_v}{2}]} \frac{J_1(m_1^j \frac{\hat{r}_v}{\hat{a}})}{J_1(m_1^j)} \left[\frac{(m_1^j)^2}{(m_1^j)^2 - 1} \right] \quad (21)$$

The subscript $()_1$ indicates that this result applies to Case 1, all vents correlated.

Case 2: All Vents Uncorrelated

When n uncorrelated pressure signals $p_i(t)$ are added, the net rms level is

$$\bar{p} = \sqrt{\sum_{i=1}^n \bar{p}_i^2} \quad (22)$$

For example, if there are only two pressure contributions

$$p^2 = (p_1(t) + p_2(t))^2 = p_1^2 + p_2^2 + 2p_1p_2 \quad (23)$$

When the time average is taken to compute the mean square, the third term on the right averages to zero since p_1 and p_2 are uncorrelated. What remains corresponds to Eq. (22) for $n = 2$.

Equation (22) cannot be applied to the FSTF configuration without some additional consideration. Although the vent sources within



Vertical text on the left margin, possibly bleed-through from the reverse side of the page.

Faint horizontal text at the top of the page.

Faint horizontal text in the upper middle section.

Faint horizontal text in the middle section.

Faint horizontal text at the bottom of the page.

the facility are uncorrelated, the rigid end walls cause each source to have a correlated image system. A single source and its correlated image system is shown schematically in Figure 5. Formally, the contribution \bar{p}_{av_i} of each source and its image system must first be found. The value of \bar{p}_{av_i} must be based on $\hat{\ell}$, the length of the entire FSTF segment. The net value of \bar{p}_{av} is then found by adding the uncorrelated contributions \bar{p}_{av_i} according to Eq. (22). This procedure, which is straightforward but tedious, can be circumvented by reasoning from a different point of view.

If a single pulsating source is placed in an infinitely long cylinder, it produces a certain net vertical force. Suppose an infinite number of sources are placed in the cylinder in a periodic pattern to form the image system shown in Figure 5, with one source per length $\hat{\ell}$. Then the net force acting on the length $\hat{\ell}$ must be the same as the net force produced by a single source on the entire tube. In particular, the force on the segment is independent of the specific source location, as long as the sources are distributed to satisfy the image pattern. The conclusion is that each source in the segment makes the same contribution \bar{p}_{av_s} independent of its location. If these sources were correlated, as in Case 1 above, their net contribution would be $8\bar{p}_{av_s}$. However, since these sources are uncorrelated, Eq. (18) gives their net contribution as $\sqrt{8}\bar{p}_{av_s}$. Since the source strength is linearly proportional to pressure, it follows that the strength of uncorrelated sources (Case 2) is

$$\bar{Q}_2 = \sqrt{8}\bar{Q}_1 = 2.8284 \bar{Q}_1 \quad (24)$$

where \bar{Q}_1 is determined using Eqs. (20) and (21).

As a check on this reasoning, the same result was obtained by the formal method described earlier. The approach is summarized below, but the detailed derivation is omitted. Equations (13) and (14) were evaluated for the case $\hat{D} \rightarrow \infty$, namely a single source in an infinitely long cylinder. The contribution of each source and image system was obtained for each subsegment $\hat{\ell}_v$. The contribution of each source on the entire segment of length $\hat{\ell}$ was



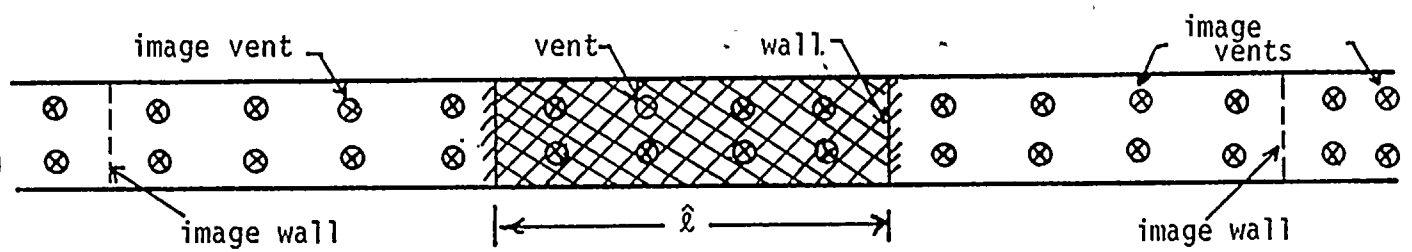


Figure 5.. FSTF Geometry for Case 2: All Vents Uncorrelated.



determined, and indeed was found to be independent of source location. Finally, the source strength was found to be given by the following expression:

$$\bar{Q}_2 = \bar{p}_x \frac{\hat{\ell}_v \hat{a}^2}{\sqrt{2} \rho \omega} \left[\sum_{s=1}^{\infty} \sum_{j=1}^{\infty} K_{j\infty} e^{-\alpha_{1j}(2s-1)\hat{\ell}_v/2} \right]^{-1} \quad (25)$$

where

$$K_{j\infty} = \frac{\sin \hat{\theta}_v}{\alpha_{1j}^2} \sinh[\alpha_{1j} \frac{\hat{\ell}_v}{2}] \frac{J_1(m_1^j \frac{\hat{r}_v}{\hat{a}})}{J_1(m_1^j)} \left[\frac{(m_1^j)^2}{(m_1^j)^2 - 1} \right] \quad (26)$$

Numerical evaluation of these expressions shows the result to be identical to Eq. (24).

PREDICTION OF VERTICAL PRESSURE IN TORUS

Case I: All Vents Correlated

This case is similar to Case 1 discussed in the previous section. As indicated in Figure 6, the correlated vents form an image system equivalent to placing rigid walls at a distance $\ell_v/2$ on each side of the vent station. Therefore, in Eqs. (13) and (14) set $D = \ell_v/2$. Evaluation of \bar{p}_{av} on the cross-hatched area is equivalent to setting $d = \ell_v/2$ and $z = \ell_v/4$. The net average vertical pressure component is thus

$$\bar{p}_{T_I} = n_v \bar{p}_{av} \left(\frac{\ell_v}{4} \right) \left| \begin{array}{l} D = \ell_v/2 \\ d = \ell_v/2 \\ \bar{Q} = \bar{Q}_1 \end{array} \right. \quad (27)$$

where \bar{p}_{av} and \bar{Q}_1 are given by Eqs. (13) and (20), respectively, and n_v is the number of vents at each station (Figure 6 shows $n_v = 2$).

A comment on using the source strengths as found in the previous section is now appropriate. The direct use of these source strengths is really only valid if the water in the vessel provides the same



A
19, 26

..



7



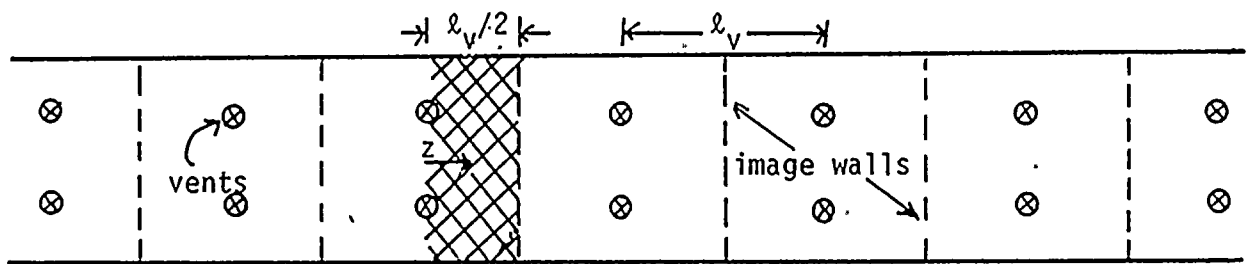


Figure 6. Unwrapped Torus Geometry for Case I: All Vents Correlated.



100
100
100
100
100

100
100
100
100
100

100
100
100
100
100

100
100

unsteady loading on the end of the vent in each case. This condition does not require that the geometry of the torus (radius, vent spacing, etc.) be identical to that of FSTF, but of course it is satisfied in that case. The point is that, in geometries that are substantially different, an additional source transfer procedure would improve accuracy. However, such a source transfer procedure cannot be readily performed without additional detailed calculations.

Case II: All Vents Uncorrelated

The geometry for this case is sketched in Figure 7. Since the vents are uncorrelated, the influence of each vent on a fixed area of the torus is first determined, and the contributions are then added according to Eq. (22). Since the torus closes on itself, half of the torus can be replaced by a reflection plane (rigid wall) directly across from the vent. Equations (17), (18) and (19) give the appropriate expression for the average vertical pressure in this case. The reflection from the plane of symmetry accounts for the second (longer) transmission path around the torus from the source to the point of evaluation. The effect of different sources on a fixed area is equivalent to the effect of a fixed source on different (equal) areas, since it is the distance between them that is important. The length over which the area averaging takes place is chosen to be $d = \ell$ the length of a segment. Referring to Eq. (17), the contribution of a source a distance $z = [s - \frac{1}{2}] \ell_v$, "s" an integer, from the center of the averaging area is $\bar{p}_{avL}([s - \frac{1}{2}] \ell_v)$. Because of the symmetry of the torus, there are two vent stations $\left. \begin{array}{l} d = \ell \\ \bar{Q} = \bar{Q}_2 \end{array} \right|$ (on opposite sides) at this distance, and there are n_v vents at each station. Adding all such contributions according to Eq. (22) gives the Case II result:

$$\bar{p}_{T_{II}} = \sqrt{2n_v \sum_{s=1}^{N_s/2} \bar{p}_{avL}^2([s - \frac{1}{2}] \ell_v)} \left. \begin{array}{l} d = \ell \\ \bar{Q} = \bar{Q}_2 \end{array} \right| \quad (28)$$

where $N_s/2$ is the number of vent stations in half of the torus ($N_s = N n_s$). The uncorrelated source strength \bar{Q}_2 is determined



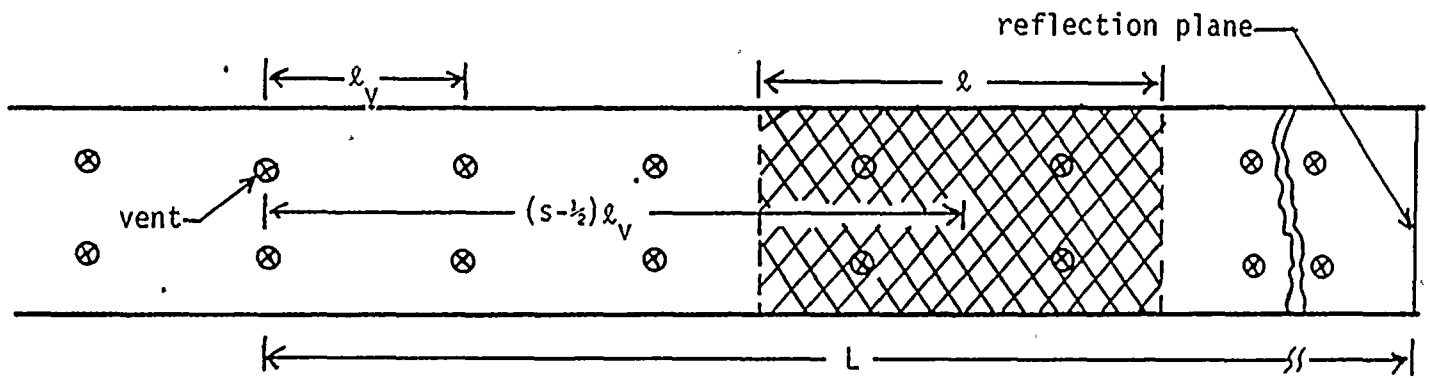


Figure 7. Unwrapped Torus Geometry for Case II:
All Vents Uncorrelated.



Vertical text or markings along the left edge of the page, possibly bleed-through from the reverse side.

by Eq. (24) or Eqs. (25) and (26).

It is also possible to arrive at a related result of some interest. The value of $\bar{p}_{T_{II}}$ averaged over the planform area of the entire torus, namely $d = 2L$, is easily deduced. A single vent produces a given net vertical force in the entire torus regardless of its location due to symmetry. This force can be found by dividing the correlated source (Case I) result by the total number of sources $N_s n_v = N n_s n_v$. However, by Eq. (24) the source strength $\bar{Q}_2 = \sqrt{8} \bar{Q}_1$ is to be used when all sources are uncorrelated. Thus, the contribution to the average vertical pressure of any one of the uncorrelated vents is $\sqrt{8} \bar{p}_{T_I} / N n_s n_v$, where the averaging area is the entire torus planform. Adding all the contributions according to Eq. (22) gives

$$\bar{p}_{T_{II} \text{ ENTIRE TORUS}} = \sqrt{\frac{8}{N n_s n_v}} \bar{p}_{T_I} \quad (29)$$

where \bar{p}_{T_I} is given by Eq. (27). Because of the lack of correlation between segments, Eq. (29) always gives a lower value than Eq. (28).

Case III: Correlated Vents in Each Segment, Segments Uncorrelated

As an intermediate case between the two just considered, suppose that the vents in each segment are correlated, but that each segment is uncorrelated from the others. The averaging area is again chosen to be $d = \ell$, the segment length. The contribution of each segment of correlated sources on the averaging area is first determined, and then these uncorrelated segment contributions are added according to Eq. (22). This approach is illustrated schematically in Figure 8. The correlated pressure from a segment centered a distance $s\ell$, $s=1, \dots, N/2-1$, away from the center of the averaging area is the sum of the individual pressures given by Eq. (17):

$$\bar{p}_s = n_v \sum_{\delta=1}^{n_s} \bar{p}_{av_L} \left(s\ell + \left[\frac{n_s+1}{2} - \delta \right] \ell \right) \Bigg|_{\substack{d=\ell \\ \bar{Q}=\bar{Q}_1}} \quad n_s \text{ even or odd} \quad (30)$$



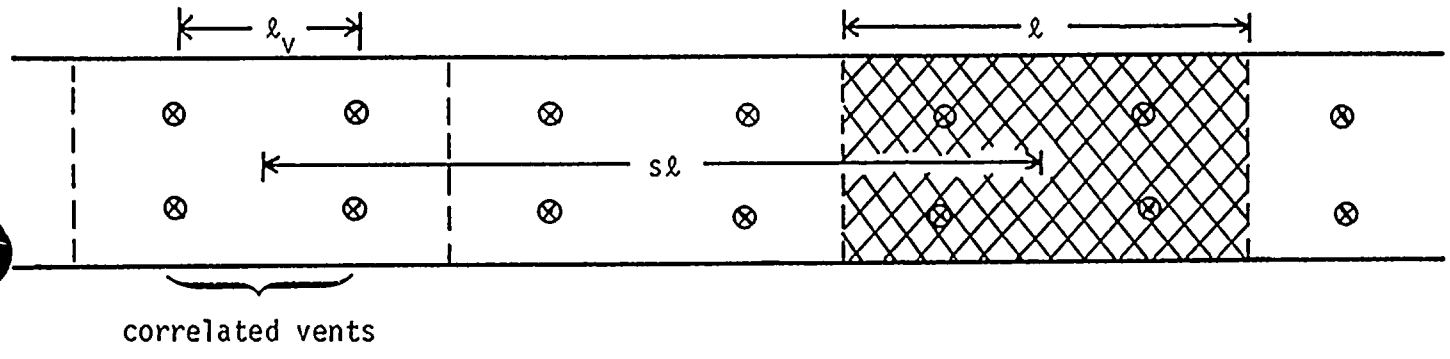


Figure 8 . Unwrapped Torus Geometry for Case III: Correlated Vents in Each Segment, Segments Uncorrelated.



Vertical text on the left side, possibly a page number or header, appearing as a column of small, illegible characters.

Main body of text, consisting of several lines of illegible characters scattered across the page.

where n_s is the number of stations in a segment and n_v is the number of vents at each station. The most reasonable choice of source strength seems to be \bar{Q}_1 since most adjacent sources are correlated and since a torus segment length is comparable to the length of FSTF. For the segment directly over the averaging area ($s=0$) the pressure is given by:

$$\bar{p}_0 = 2n_v \sum_{\delta=1}^{n_s/2} \bar{p}_{av_L}([\delta - \frac{1}{2}]l_v) \Big|_{\substack{d=l \\ \bar{Q}=\bar{Q}_1}} \quad n_s \text{ even} \quad (31)$$

Similarly, for the segment directly opposite the averaging area ($s = N/2$) the pressure is

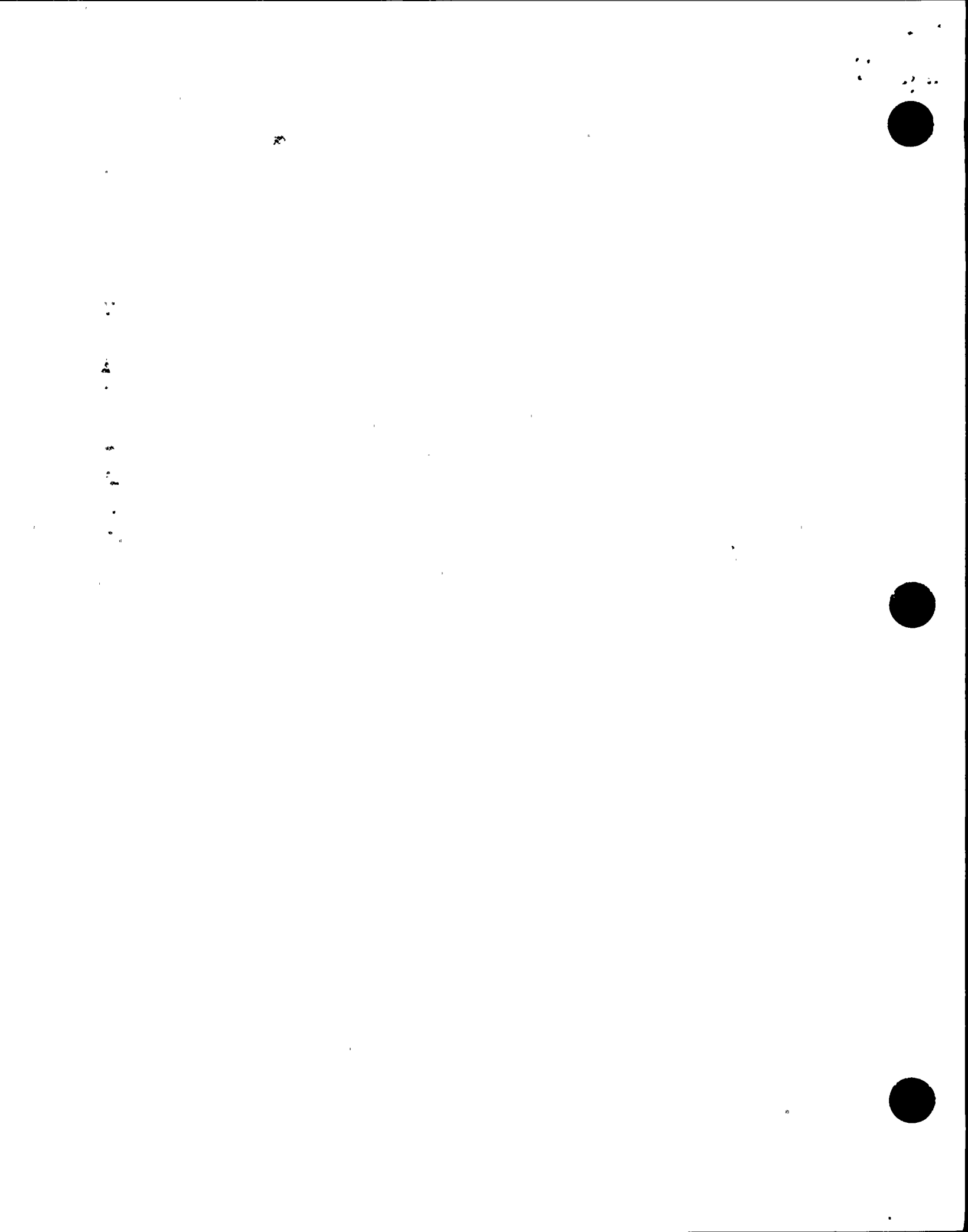
$$\bar{p}_{N/2} = 2n_v \sum_{\delta=1}^{n_s/2} \bar{p}_{av_L}(L - [\delta - \frac{1}{2}]l_v) \Big|_{\substack{d=l \\ \bar{Q}=\bar{Q}_1}} \quad n_s \text{ even} \quad (32)$$

Similar expressions for \bar{p}_0 and $\bar{p}_{N/2}$ may be derived for n_s odd. The special forms of Eq. (31) and (32) are necessary because the restriction $0 \leq z \leq L$ applies to Eq. (17). Because of the symmetry of the torus, the contribution of half the sources (those located within $0 \leq z \leq L$) can be doubled. Adding these uncorrelated pressures given the Case III result:

$$\bar{p}_{T_{III}} = \sqrt{\bar{p}_0^2 + 2 \sum_{s=1}^{(N-2)/2} \bar{p}_s^2 + \bar{p}_{N/2}^2} \quad (33)$$

The factor of two before the summation sign accounts for the fact that there are two uncorrelated segments of equal distance on either side of the averaging area. Since Case III is a reduction in the degree of correlation as compared to Case I, Eq. (27), the following inequality always holds: $\bar{p}_{T_{III}} < \bar{p}_{T_I}$.

The related result for which the torus planform is the averaging area is easily deduced. The net vertical pressure of a single vent in the torus is the Case I result divided by the total number of



sources, namely $\bar{p}_{T_I} / N n_s n_v$. The net pressure due to a segment having $n_s n_v$ correlated sources is therefore \bar{p}_{T_I} / N . Using Eq. (22) to add N such equal uncorrelated levels to account for all the segments gives

$$\bar{p}_{T_{III}}^{\text{ENTIRE TORUS}} = \frac{1}{\sqrt{N}} \bar{p}_{T_I} \quad (34)$$

Because the individual segments are uncorrelated, the level given by Eq. (34) is always less than that given by Eq. (33). Interestingly, comparing Eqs. (29) and (34), the Case II and III levels for the entire torus, shows these levels to be comparable although Case III should be higher. This reflects the fact that the choice of Q_1 for the source strength in Case III is an approximation and that the value for a partially correlated case actually should be used.

IV. CALCULATION OF THE PSD LOAD REDUCTION FACTORS IN FSTF

The FSTF downcomer pressures have been shown earlier to be nearly uncorrelated in the 0 - 50 Hz frequency range, (except at 5 Hz and in the frequency range 8 - 10 Hz). The analysis then shows that for all of the vents uncorrelated within the bay, Eqs. (24), (20), and (21) are needed to determine the vent source strength, given the FSTF geometry. Once this source strength is obtained, the analysis for all vents uncorrelated, including the effects of all uncorrelated (image) bays, Eq. (28), results in the net average vertical pressure in a prototypical plant. It is the purpose of this section to calculate the PSD reduction factors available by this analysis, before discussing the effect of partial correlation.

For the FSTF geometry, the normalized source strength for Case 2 may be determined by defining the quantity

$$\bar{q} = \frac{\rho \omega \sin \hat{\theta}_v \bar{Q}_2}{2 \hat{\ell}_v \hat{a}^2 \bar{p}_x} \quad (35)$$

so that

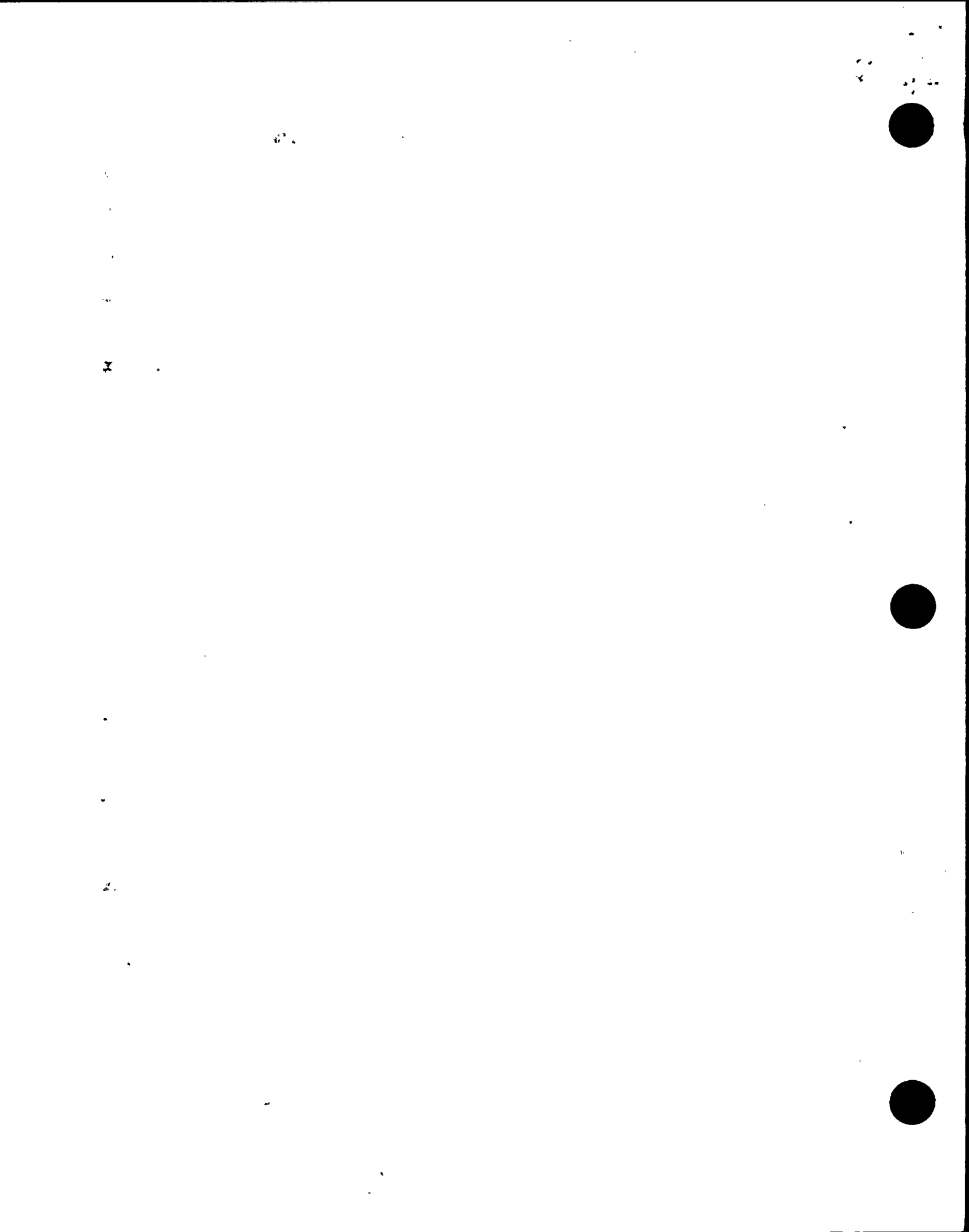
$$\bar{q} = \left[\sqrt{8} \sum_{j=1}^{\infty} K_j \cosh[\alpha_{1j} \frac{\hat{\ell}_v}{4}] \right]^{-1} \quad (36)$$

with

$$K_j = \frac{1}{\alpha_{1j}^2} \frac{\sinh[\alpha_{1j} \frac{\hat{\ell}_v}{4}] J_1(m_1^j \frac{\hat{r}_v}{\hat{a}})}{\sinh[\alpha_{1j} \frac{\hat{\ell}_v}{2}] J_1(m_1^j)} \left[\frac{(m_1^j)^2}{(m_1^j)^2 - 1} \right] \quad (37)$$

$$\alpha_{1j} = \frac{1}{a} \sqrt{(m_1^j)^2 - \left(\frac{\omega a}{c}\right)^2} \quad (38)$$

and m_1^j is the zeros of the slope of J_1 . Equations (36) and (37) are a rewriting of Eqs. (24), (20) and (21) appropriate for the definition in Eq. (35). Using these equations, the vent source strength \bar{q} may be obtained; \bar{q} is a function of the plant



geometry, frequency ω and sound speed c .

An application of Eqs. (13), (14), (17)-(19) and (28) to the equivalent FSTF plant (where $\hat{\ell} = 2\hat{\ell}_v$) yields the resultant average vertical pressure for Case II as

$$\frac{\bar{p}_{TII}}{\bar{p}_x} = \bar{q} \sqrt{2\hat{n}_v \sum_{s=1}^{\hat{N}_s/2} \hat{p}_{avL}^2 ([s-\frac{1}{2}]\hat{\ell}_v)} \quad (39)$$

where \bar{p}_x is the experimentally determined pressure and

$$\hat{p}_{avL}(\eta) = \begin{cases} \hat{p}_{av}(\frac{\hat{d}}{2}) \Big|_{\hat{d}=\hat{\ell}_v+\eta} + \hat{p}_{av}(\frac{\hat{d}}{2}) \Big|_{\hat{d}=\hat{\ell}_v-\eta} & 0 \leq \eta < \hat{\ell}_v \\ \hat{p}_{av}(\eta) \Big|_{\hat{d}=2\hat{\ell}_v} & \hat{\ell}_v \leq \eta \leq \hat{L}-\hat{\ell}_v \\ \hat{p}_{av}(\hat{L}-\frac{\hat{d}}{2}) \Big|_{\hat{d}=\hat{\ell}_v+\hat{L}-\eta} + \hat{p}_{av}(\hat{L}-\frac{\hat{d}}{2}) \Big|_{\hat{d}=\hat{\ell}_v-\hat{L}+\eta} & \hat{L}-\hat{\ell}_v < \eta \leq \hat{L} \end{cases} \quad (40)$$

$$\hat{p}_{av}(\eta) = \sum_{j=1}^{\infty} \hat{K}_j \cosh[\alpha_{1j}(\hat{L}-\eta)] \quad (41)$$

$$\hat{K}_j = \frac{1}{\alpha_{1j}^2} \frac{\sinh(\alpha_{1j} \frac{\hat{d}}{2})}{\sinh(\alpha_{1j} \hat{L})} \frac{J_1(m_1^j \frac{\hat{r}_v}{\hat{a}})}{J_1(m_1^j)} \left[\frac{(m_1^j)^2}{(m_1^j)^2 - 1} \right] \quad (42)$$

For the FSTF geometry,

$$\begin{aligned} \hat{n}_s &= 4 \\ \hat{n}_v &= 2 \\ \hat{N}_s &= 64 \\ \hat{\ell} &= 9.75 \text{ ft } (\hat{\ell}_v = 4.88 \text{ ft}) \\ \hat{a} &= 13.83 \text{ ft} \\ \hat{r}_v &= 7.21 \text{ ft } (\hat{\theta}_v = 56.3^\circ) \\ \hat{L} &= 156 \text{ ft} \end{aligned}$$



The square of the results of Eq. (39) yields the PSD reduction factors shown in Figure 9. Although the curves begin at 0 Hz, the reduction factor is strictly valid only in the frequency range where the sources are random and uncorrelated. The results are a function of the sound speed c and a function of frequency. The reduction factor is always less than 0.53.



P.S.D. Load Reduction Factor

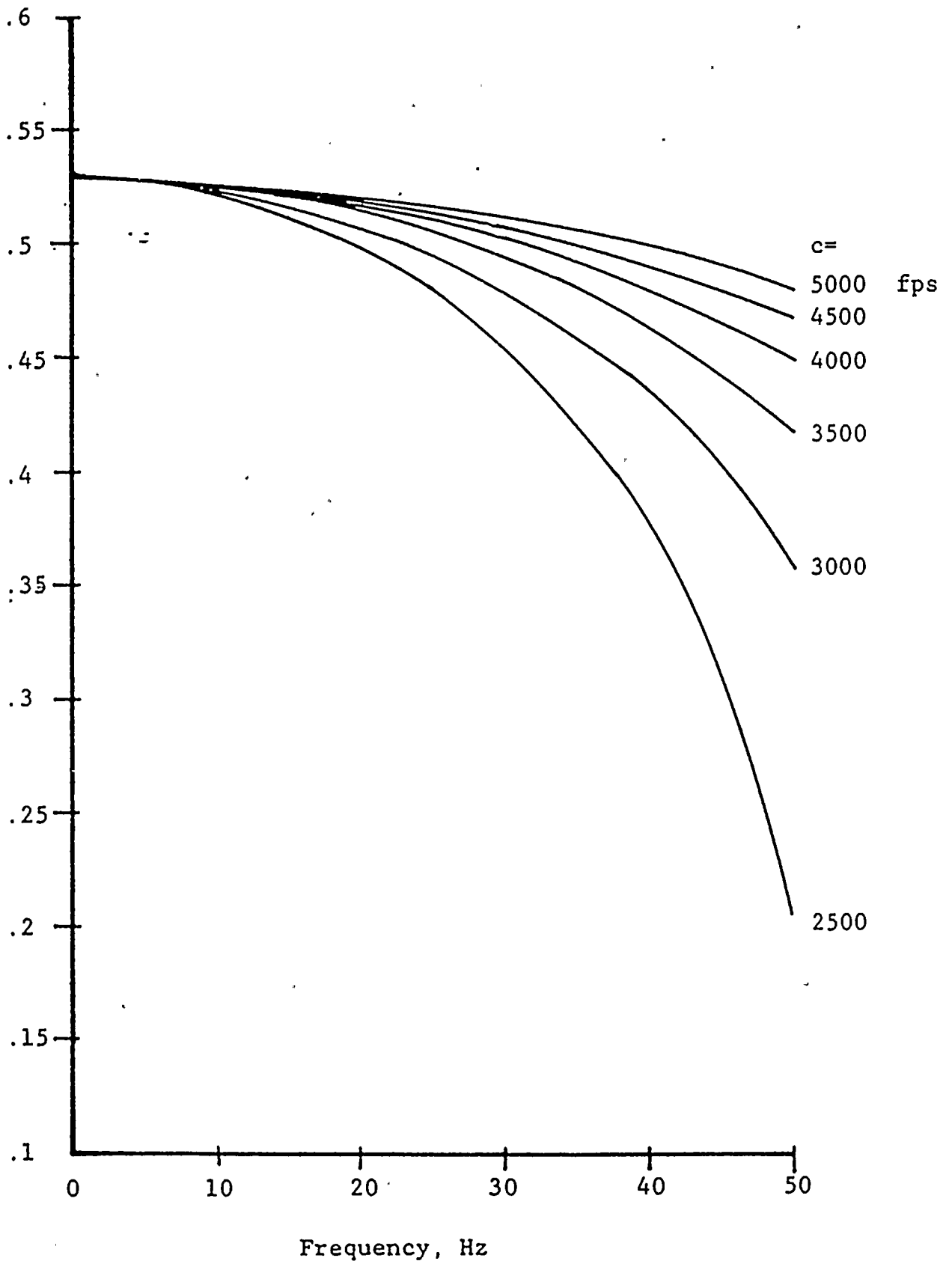


Figure 9: P.S.D. Reduction factor as a function of frequency for Uncorrelated Vents Case II in FSTF.

12
3
4
5
6
7
8
9
10
11
12
13
14
15
16
17
18
19
20
21
22
23
24
25
26
27
28
29
30
31
32
33
34
35
36
37
38
39
40
41
42
43
44
45
46
47
48
49
50
51
52
53
54
55
56
57
58
59
60
61
62
63
64
65
66
67
68
69
70
71
72
73
74
75
76
77
78
79
80
81
82
83
84
85
86
87
88
89
90
91
92
93
94
95
96
97
98
99
100

V. EFFECT OF PARTIAL CORRELATION BETWEEN VENTS

GENERAL APPROACH

So far in this report we have considered primarily the cases of perfect correlation or perfect uncorrelation between vents. In this section we examine the theoretical and practical limitations of partial correlation between vents.

The multivalent FSTF/Plant configuration may be thought of as a linear system in which many time dependent inputs give a single time dependent output. The inputs in this case are the unsteady pressures in the steam vents. The linear system transfers these pressures to volume flow fluctuations at the ends of the vents and then converts these into averaged pressure fluctuations on the bottom of the torus. The output is the net fluctuating area-averaged pressure on a specified portion of the torus.

The frequency response function in the i^{th} vent will be denoted by $H_i(\omega)$. The power spectral density of the input at the i^{th} vent will be denoted by $S_{ii}(\omega)$, while the cross-spectral density of the i^{th} and j^{th} vent will be denoted by $S_{ij}(\omega)$. The frequency response functions $H_i(\omega)$ depend on configuration geometry, size of the averaging area, and distance of the i^{th} vent from the averaging area. The notation $()^*$ will denote the complex conjugate. Thus, the power spectral density of the output is given formally by ¹

$$S_T(\omega) = \sum_{i=1}^N \sum_{j=1}^N H_i^*(\omega) H_j(\omega) S_{ij}(\omega) \quad (43)$$

The frequency response functions $H_i(\omega)$ may be assumed known. The transfer function between the vent volume source and the averaged bottom pressure was determined earlier in this report. (See Equations 13-15 and 17-19 for the result in general form). The transfer function between internal vent pressure and volume flow is actually not known (and really may not be entirely linear). However, since this function is the same in every vent,

¹D.E. Newland, Random Vibrations and Spectral Analysis, Publisher: Longman, 1975. Chapter 7, Eq.(7.14) page 72.



Vertical text on the left side, possibly a page number or header.

Vertical text on the left side.

Main body of text, appearing as faint horizontal lines across the page.

and since ultimately the FSTF pressure data is used to infer torus pressures, this part of the frequency response function effectively cancels out.

The important point to observe in Eq. (43) is that to compute $S_T(\omega)$ in general requires a knowledge of not only all the spectral densities, but also all the cross-spectral densities. While it may reasonably be assumed that all the spectral densities $S_{ii}(\omega)$ are identical, such an assumption may not in general be applied to the cross-spectral densities. The cross-spectral density is given by the transform of the cross-correlation function:

$$S_{ij}(\omega) = \frac{1}{2\pi} \int_{-\infty}^{+\infty} R_{ij}(\tau) e^{i\omega\tau} d\tau \quad (44)$$

where

$$R_{ij}(\tau) = \overline{p_i(t)p_j(t+\tau)} \quad (45)$$

for input pressures $p(t)$.

The correlation coefficient for any two vents is defined as

$$\rho_{ij} = \frac{\overline{p_i(t)p_j(t)}}{\sqrt{\overline{p_i^2(t)} \overline{p_j^2(t)}}} = \frac{R_{ij}(0)}{\sqrt{\overline{p_i^2(t)} \overline{p_j^2(t)}}} \quad (46)$$

where $-1 \leq \rho_{ij} \leq 1$. Notice that specifying all the correlation coefficients does not in general provide enough information to calculate $S_T(\omega)$. In fact, two sets of inputs which are fundamentally different may have the same correlation coefficient but different cross-spectra, and thus produce a different system output. However, the correlation coefficient is useful when narrow frequency bands are considered, as will be discussed later.

RELATION TO RESULTS IN PREVIOUS SECTIONS

Earlier in the report, results were computed for two limiting cases of interest. In Case I all the vent pressures

100



100

100

100

100

100

100

100

100

100

100

100

100

100

100

100

100

100

100

100

100

100

100

100

100

100

100

100

100

100

100

100

100

100

100

100

100

100

100

100

100



have identical time histories, so that all the spectra and cross-spectra are identical, namely $S_{ii}(\omega) = S_{ij}(\omega)$ for all i and j . Independent of this assumption, we may always write

$$H_i(\omega) = F(\omega)\hat{H}_i(\omega) \quad (47)$$

Here $F(\omega)$ is the complex transfer function across the vent steam/water interface, which is the same for all vents. The function $\hat{H}_i(\omega)$ is the transfer function from the vent to the torus wall; from Eq. (19), $\hat{H}_i(\omega) = \bar{P}_{avL}/\bar{Q}$. The analysis has shown that $\hat{H}_i(\omega)$ is real for frequencies below the acoustic cut-off frequency for the torus. The power spectral density of the pressure on the torus becomes:

$$S_T(\omega) = S_{11}(\omega) |F(\omega)|^2 \sum_{i=1}^N \sum_{j=1}^N \hat{H}_i(\omega)\hat{H}_j(\omega) \quad (48)$$

The double summation may be re-expressed to give the result

$$S_{T_I}(\omega) = S_{11}(\omega) |F(\omega)|^2 \left\{ \sum_{i=1}^N \hat{H}_i(\omega) \right\}^2 \quad (49)$$

Equation (49) is the equivalent of the result for all vents perfectly correlated, called Case I and given by Eq. (27). The actual Case I result was obtained in a different and more convenient way by using an image method.

The other result obtained previously was for all vent pressures perfectly uncorrelated, namely $R_{ij}(\tau) = 0$ and $S_{ij}(\omega) = 0$ whenever $i \neq j$. All vent pressures were assumed to have identical power spectral densities, namely $S_{11}(\omega) = S_{ii}(\omega)$ for all i . Then Eq. (49) becomes

$$S_{T_{II}}(\omega) = S_{11}(\omega) |F(\omega)|^2 \sum_{i=1}^N \hat{H}_i^2(\omega) \quad (50)$$

This result is equivalent to the Case II result of Eq. (28), obtained by performing a summation equivalent to that given by Eq. (50).

Earlier in the report, the factor corresponding to $S_{11}(\omega) |F(\omega)|^2$ which appears in both Eqs. (49) and (50) was related to the wall pressures measured in FSTF for the cases of perfectly correlated and perfectly uncorrelated vents. It was then possible to predict torus wall pressures in terms of FSTF wall pressures. The torus diameter and vent geometry were assumed to be the same as in FSTF. Then if all sources are perfectly correlated, the wall pressures in the torus are the same as in FSTF. However, if all sources are uncorrelated, the wall pressures in the torus are lower than those in FSTF because the rigid end walls in FSTF produce correlated image sources. It was, therefore, possible to plot a power spectral density reduction factor as a function of frequency to show the effect of perfectly uncorrelated vent sources, Fig. 9.

EFFECT OF PARTIAL CORRELATION

When some degree of correlation exists between the input pressures from various vents, the problem becomes much more difficult. Equation (43) shows that all the cross-spectral densities in the torus must be known. These cannot be obtained from FSTF, except perhaps for adjacent vents. In particular, specifying just the correlation coefficients is not in general adequate unless the data is analyzed in narrow frequency bands. Even so, it is necessary to specify all the pairs of correlation coefficients. In the following analysis, the correlation coefficients of all possible vent pairs are assumed to be equal.

The spectral density and correlation function are a Fourier transform pair; thus, corresponding to Equation (44),

$$R_{ij}(\tau) = \int_{-\infty}^{+\infty} S_{ij}(\omega) e^{i\omega\tau} d\omega \quad (51)$$

It follows that for a very narrow bandwidth, $\Delta\omega$, the correlation function is approximately

$$R_{ij}(\tau) \approx S_{ij}(\omega) e^{i\omega\tau} \Delta\omega \quad (52)$$

where ω is interpreted as the band center frequency. Then

$$R_{ij}(0) = S_{ij}(\omega) \Delta\omega \quad (53)$$

Equation (46) may be rewritten first using Equation (45) and then Equation (53), to give

$$\rho_{ij} = \frac{R_{ij}(0)}{\sqrt{R_{ii}(0)R_{jj}(0)}} = \frac{S_{ij}(\omega)}{\sqrt{S_{ii}(\omega)S_{jj}(\omega)}} \quad (54)$$

Assuming that all vents have the same power spectral density gives

10
11
12
13
14
15
16
17
18
19
20
21
22
23
24
25
26
27
28
29
30
31
32
33
34
35
36
37
38
39
40
41
42
43
44
45
46
47
48
49
50
51
52
53
54
55
56
57
58
59
60
61
62
63
64
65
66
67
68
69
70
71
72
73
74
75
76
77
78
79
80
81
82
83
84
85
86
87
88
89
90
91
92
93
94
95
96
97
98
99
100



1
2
3
4
5
6
7
8
9
10
11
12
13
14
15
16
17
18
19
20
21
22
23
24
25
26
27
28
29
30
31
32
33
34
35
36
37
38
39
40
41
42
43
44
45
46
47
48
49
50
51
52
53
54
55
56
57
58
59
60
61
62
63
64
65
66
67
68
69
70
71
72
73
74
75
76
77
78
79
80
81
82
83
84
85
86
87
88
89
90
91
92
93
94
95
96
97
98
99
100

1
2
3
4
5
6
7
8
9
10
11
12
13
14
15
16
17
18
19
20
21
22
23
24
25
26
27
28
29
30
31
32
33
34
35
36
37
38
39
40
41
42
43
44
45
46
47
48
49
50
51
52
53
54
55
56
57
58
59
60
61
62
63
64
65
66
67
68
69
70
71
72
73
74
75
76
77
78
79
80
81
82
83
84
85
86
87
88
89
90
91
92
93
94
95
96
97
98
99
100

$$S_{ii}(\omega) = S_{jj}(\omega) \equiv S_{11}(\omega) \quad i=j \quad (55)$$

The cross-spectral density is assumed to be the same between all vent pairs, so that for all i and j , not equal,

$$S_{ij}(\omega) \equiv S_c(\omega) \quad i \neq j \quad (56)$$

Equations (55) and (56) represent the only assumptions that can reasonably be made without full scale tests on a complete torus geometry. Equations (54), (55) and (56) give

$$\rho_{ij} = \frac{S_{ij}(\omega)}{S_{ii}(\omega)} \quad (57)$$

which may also be expressed as

$$\rho_{ij} = \begin{cases} 1 & i=j \\ \rho_c & i \neq j \end{cases} \quad (58)$$

where

$$\rho_c \equiv \frac{S_c(\omega)}{S_{11}(\omega)} \quad (59)$$

The correlation coefficient ρ_c is common to all vent pairs.

It is now possible to find the load reduction factor as a function of ρ_c . The cases $\rho_c = 1$ and $\rho_c = 0$ have already been worked out when the FSTF and torus segment geometries are identical. There is no reduction for identical geometries when $\rho_c = 1$; Fig.9 gives the case $\rho_c = 0$. The power spectral density of the output is found by combining Equations (43), (47), (55) and (57):

$$S_T(\omega) = S_{11}(\omega) |F(\omega)|^2 \sum_{i=1}^N \sum_{j=1}^N \rho_{ij} \hat{H}_i(\omega) \hat{H}_j(\omega) \quad (60)$$

Next, using Equations (58) and rearranging the summation operations gives

02
12
00



$$S_T(\omega) = S_{11}(\omega) |F(\omega)|^2 \left[\rho_c \left(\sum_{i=1}^N \hat{H}_i(\omega) \right)^2 + (1-\rho_c) \sum_{i=1}^N \hat{H}_i^2(\omega) \right] \quad (61)$$

A corresponding result applies to the FSTF geometry, where the transfer functions are now denoted by $\tilde{H}_i(\omega)$:

$$S_{FSTF}(\omega) = S_{11}(\omega) |F(\omega)|^2 \left[\rho_c \left(\sum_{i=1}^8 \tilde{H}_i(\omega) \right)^2 + (1-\rho_c) \sum_{i=1}^8 \tilde{H}_i^2(\omega) \right] \quad (62)$$

where there are eight vents in FSTF.

The reduction factor of the torus pressure loads as compared to the FSTF loads is defined as

$$R_F(\rho_c, \omega) = \frac{S_T(\omega)}{S_{FSTF}(\omega)} \quad (63)$$

Substituting Equations (61) and (62) into the above then gives

$$R_F(\rho_c, \omega) = \frac{K_G \rho_c + (1-\rho_c) K_F K_C}{\rho_c + (1-\rho_c) K_C}$$

where

$$K_G = \frac{\left(\sum_{i=1}^N \hat{H}_i \right)^2}{\left(\sum_{i=1}^8 \tilde{H}_i \right)^2} \quad (64)$$

and

$$K_C = \frac{\sum_{i=1}^8 \tilde{H}_i^2}{\left(\sum_{i=1}^8 \tilde{H}_i \right)^2} \quad (65)$$

and

$$K_F = \frac{\sum_{i=1}^N \hat{H}_i^2}{\sum_{i=1}^8 \tilde{H}_i^2} \quad (66)$$

The above three constants have a simple physical interpretation.

Handwritten marks and symbols in the top right corner.



Vertical text on the left side, possibly a page number or header.

Vertical text on the left side, possibly a page number or header.

Vertical text on the left side, possibly a page number or header.

Vertical text on the left side, possibly a page number or header.

Vertical text on the left side, possibly a page number or header.

Vertical text on the left side, possibly a page number or header.

Vertical text on the left side, possibly a page number or header.



By considering the limit $\rho_c = 1$, the constant K_G is seen to reflect the difference between the FSTF segment geometry and the torus segment geometry. It is, in fact, the ratio of mean square torus pressure to the mean square FSTF pressure when all sources are perfectly correlated in both cases. It is the square of the ratio of the Case I and Case 1 pressure results obtained earlier in this report. When the segment geometries are identical, as they are assumed to be in the calculations to obtain Fig. 9, $K_G = 1.0$.

The factor K_c is the ratio of the uncorrelated to correlated mean square pressures in FSTF given identical volume source strengths. Alternatively, it is the square of the ratio of the correlated to uncorrelated volume flow strengths, \bar{Q} , given the same pressure in both cases. From Equation (24), $K_c = 1/8$.

Finally, the factor $K_F = R_F(0, \omega)$, as can be seen by setting $\rho_c = 0$. Since $R_F(0, \omega)$ is just the reduction factor for all sources uncorrelated, it may be read directly from Fig. 9. Note, however, that Fig. 9 may be used only for identical segment geometries of the torus and FSTF, i.e., only when $K_G = 1$. New results for $R_F(0, \omega)$ must first be computed if the segment geometries are different.

Thus, for the purposes of this report, the power spectral density reduction factor takes on a relatively simple form:

$$R_F(\rho_c, \omega) = \frac{\rho_c + \frac{(1-\rho_c)R_F(0, \omega)}{8}}{\rho_c + \frac{(1-\rho_c)}{8}} \quad (67)$$

In the next paragraph, it is suggested that the restriction $0 \leq \rho_c \leq 1$ apply to this equation. This load reduction factor is plotted in Fig. 10 for several values of ρ_c assuming $c = 2500$ ft/sec. It may be seen that small values of ρ_c quickly increase the load reduction factor above the uncorrelated value $R_F(0, \omega)$.

Finally, the range of admissible values of ρ_c must be discussed. The only range of possible physical interest is $-1 \leq \rho_c \leq 1$.

14
13
12
11
10
9
8
7
6
5
4
3
2
1



P.S.D. Load Reduction Factor

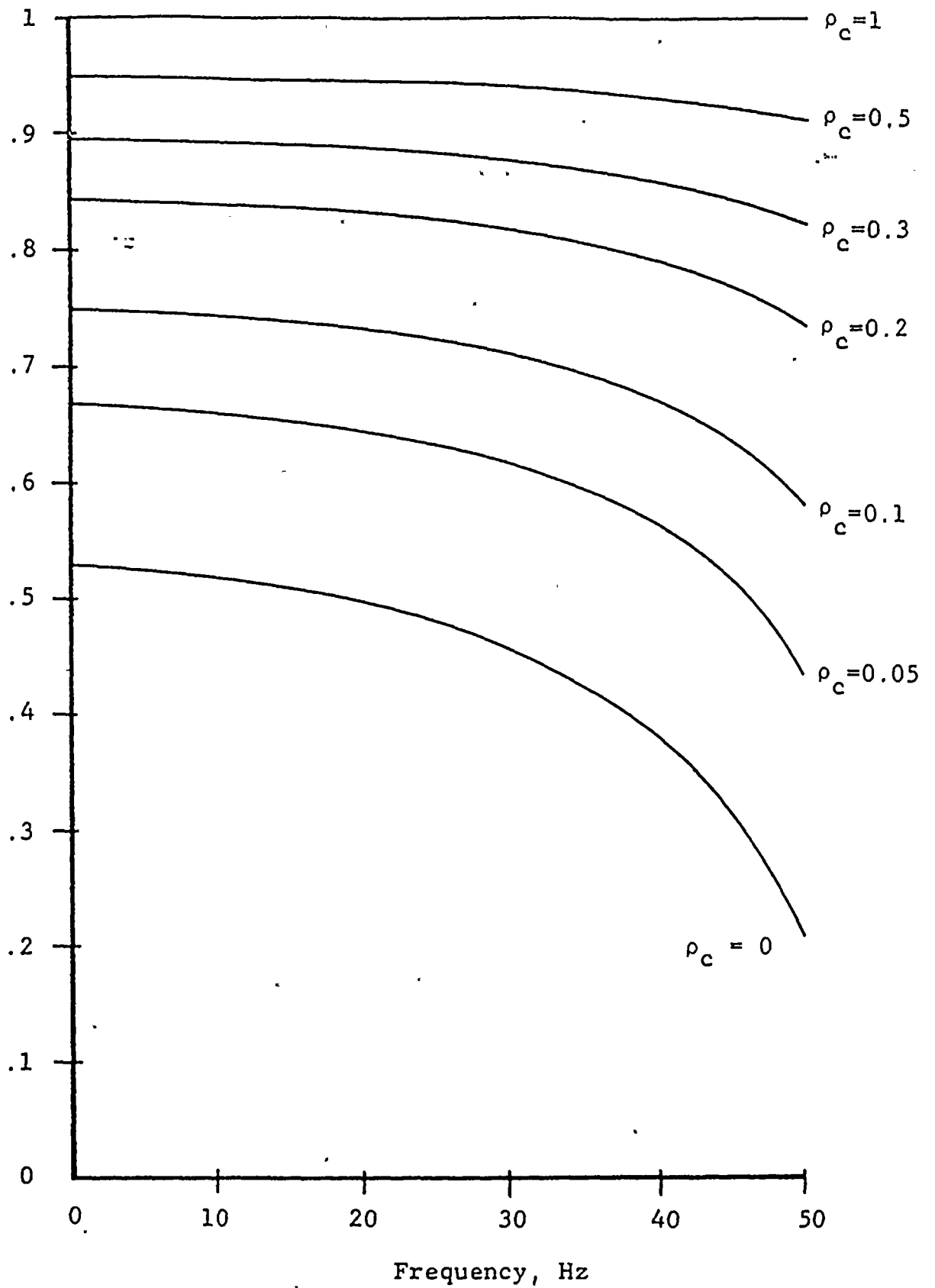


Figure 10: P.S.D. reduction factor as a function of frequency and correlation coefficient for an acoustic speed $c = 2500$ fps.

100



100

However, a further restriction is necessary. The function $R_F(\rho_c, \omega)$ given by Equation (67) approaches minus infinity as $\rho_c \rightarrow -1/7$ from above. Negative reduction factors for the power spectral density are clearly meaningless. For larger values of ρ_c , the function increases monotonically. At $\rho_c = -R_F(0, \omega)/(8 - R_F(0, \omega))$, the reduction factor $R_F(\rho_c, \omega) = 0$. This behavior reflects the fact that it is not physically realistic to assume that all correlation coefficients are equal and negative. For instance, assuming $\rho_c = -1$ implies that all vent pair combinations are out of phase, which is physically impossible. Thus, although the analysis shows a value of ρ_c for which the reduction factor is zero, this result is suspect. It should be noted that very small reduction factors can also be achieved by judicious phasing of sources, in which case ρ_c is not the same for all vent pairs. In practice, however, these possibilities are too specific to warrant inclusion in an analysis of realistic reduction factors. Thus, Equation (67) should carry the restriction $0 \leq \rho_c \leq 1$.

10
11
12
13
14
15
16
17
18
19
20
21
22
23
24
25
26
27
28
29
30
31
32
33
34
35
36
37
38
39
40
41
42
43
44
45
46
47
48
49
50
51
52
53
54
55
56
57
58
59
60
61
62
63
64
65
66
67
68
69
70
71
72
73
74
75
76
77
78
79
80
81
82
83
84
85
86
87
88
89
90
91
92
93
94
95
96
97
98
99
100

